Journal of Power Sources 196 (2011) 7847–7853

Contents lists available at ScienceDirect

Journal of Power Sources

journal homepage: www.elsevier.com/locate/jpowsour

Enhanced manganese dioxide supercapacitor electrodes produced by electrodeposition

Andrew Cross[a], Alban Morel[b], Ariana Cormie[a], Tony Hollenkamp[c], Scott Donne[a,*]

[a] Discipline of Chemistry, University of Newcastle, Callaghan, NSW 2308, Australia
[b] LGMPA, Polytech Nantes, BP50609 – rue Christian Pauc, Nantes Cedex 3, 44306, France
[c] CSIRO Division of Energy Technology, Box 312, Clayton South, VIC 3169, Australia

ARTICLE INFO

Article history:
Received 23 February 2011
Received in revised form 20 April 2011
Accepted 20 April 2011
Available online 30 April 2011

Keywords:
Manganese dioxide
Electrodeposition
Supercapacitors

ABSTRACT

Electrodeposited thin films of manganese dioxide, prepared using chronoamperometry on a platinum substrate in an electrolyte of $MnSO_4$ in H_2SO_4, possess a significantly higher capacitance compared to the literature materials (>2000 F g^{-1} which is at least a 250% increase in performance) when cycled over a 0.8 V potential window in an aqueous electrolyte of 0.5 M Na_2SO_4. This excellent performance is discussed in terms of the manganese dioxide electrodeposition mechanism, in particular the growth mechanism under the preferred slow mass transport of electro-active species, and its effects on morphology. Furthermore, the origin of the enhanced capacitance is discussed, in which case we have proposed arises from contributions made by hydroxyl groups on the manganese dioxide nano-particulate surface, in addition to the fast redox reactions that are necessary for pseudo-capacitance.

1. Introduction

One of the greatest challenges modern society faces is the efficient supply of energy. Currently most energy is produced in fossil fuel (coal, oil and natural gas) burning power stations, which unfortunately are major contributors to environmental greenhouse gas emissions. Considerable effort has been expended recently in the development and expansion of more renewable forms of energy generation such as hydroelectric, solar, geothermal, wind, biomass, etc. However, with current technologies none of these more renewable sources has the realistic ability to economically substitute for fossil fuel based power [1]. Therefore, energy production in the future is anticipated to be more distributed and intermittent in nature to capitalize on these smaller scale renewable forms of energy.

With energy production heading in such a direction, the importance of energy storage is also growing for load-levelling applications, as well as a means to improve efficiency. Various energy storage options exist, particularly when stored as chemical energy, in which case batteries, supercapacitors and fuel cells are the alternatives. Mechanical or thermal energy storage is a possibility; however, this is low grade energy, as opposed to electrochemical energy storage which produces high grade electrical energy [1].

The relative merits of batteries, supercapacitors and fuel cells can be summarized by a Ragone diagram [2]. In summary, fuel cells provide the highest energy density at the expense of power density, while the performance of supercapacitors is essentially the opposite. Batteries generally occupy an intermediate region within the Ragone plot, providing higher energy density compared to supercapacitors and greater power density compared to fuel cells. Extensive research is ongoing globally to boost the performance of each power sources, as well as to identify their preferred applications.

1.1. Supercapacitor systems

The underlying basis of our research is to boost supercapacitor energy density, and by doing so make them more broadly applicable as power sources. Commercially available supercapacitors are symmetrical devices (identical electrodes) employing activated carbon electrodes with either an aqueous (e.g., H_2SO_4) or non-aqueous (e.g., tetra alkyl ammonium tetrafluorobroate in acetonitrile) based electrolytes [3]. The performance of these devices is quite good, with high power density and long cycle life; however, as mentioned, their energy density is limited. A strategy for improving supercapacitor energy density is to incorporate a pseudo-capacitive electrode [4]; i.e., one that can store charge in the double layer, as well as undergo fast reversible surface redox reactions. These electrodes have enhanced capacity as a result of the faradaic contribution, as well as a higher density meaning that their volumetric energy density is also improved.

* Corresponding author. Tel.: +61 2 4921 5477; fax: +61 2 4921 5472.
E-mail address: scott.donne@newcastle.edu.au (S. Donne).

0378-7753/$ – see front matter © 2011 Elsevier B.V. All rights reserved.
doi:10.1016/j.jpowsour.2011.04.049

The prototypical supercapacitor electrode material is amorphous hydrated ruthenium dioxide ($RuO_2{\cdot}xH_2O$) which has been reported to have a capacitance exceeding 900 F g^{-1} in an aqueous H_2SO_4 electrolyte [5]. What primarily limits its commercial implementation is cost, which has prompted the search for suitable alternatives with similar behaviour. Alternative systems based on other metal oxides and conductive polymers have been reported in the literature to behave similarly; however, of these, metal oxides are preferred because of their higher energy density [4,5]. Within the category of metal oxides, systems based on manganese dioxide are presently receiving considerable attention from the scientific community [6]. With a myriad of available synthesis methods [7–14], and as a result wide ranging morphologies, coupled with good faradaic electrochemical performance, low cost and environmental friendliness, this class of materials represents an interesting and promising area of research.

What we are reporting on here is the excellent performance of electrodeposited thin films of manganese dioxide in aqueous electrolytes. One of the main reasons we have chosen to study electrodeposited materials is because of the inherent processing advantages they possess compared to conventional powder processing routes, in addition to the high performance nature of the materials produced.

2. Experimental methods

2.1. Materials

The main materials used in this work were $MnSO_4{\cdot}H_2O$ (Sigma Aldrich; 99.5%), concentrated H_2SO_4 (Sigma Aldrich; 98%), and Na_2SO_4 (Sigma–Aldrich; 99%). All solutions from these chemicals were made up using Milli-Q ultra pure water (>18 MΩ resistance). Manganese dioxide electrodeposition was carried out from a matrix of electrolytes covering the compositional range 0.001–1.0 M Mn^{2+} and 0.0–1.0 M H_2SO_4. To evaluate the performance of the electrodeposited manganese dioxide samples as supercapacitor electrodes an electrolyte of 0.5 M Na_2SO_4 was used.

2.2. Electrochemical cell and protocols

The cell used for electrodeposition consisted of a 250 mL glass beaker with a machined PTFE lid. The electrodes used were an epoxy body platinum disk working electrode (1.325 cm^2), a carbon rod counter electrode (area = 6.3 cm^2), and a saturated calomel reference electrode (SCE) with which all potentials are reported with respect to unless otherwise stated. Most experiments were conducted at ambient temperature (22.0 ± 0.5 °C); however, a few experiments were conducted at either 0.0 ± 0.5 °C in an ice-water bath, or at elevated temperatures through the use of a thermostat-controlled heating jacket (±1 °C).

Prior to electrodeposition the platinum electrode was firstly chemically cleaned in a bath of acidic hydrogen peroxide (0.1 M H_2SO_4 + 10% H_2O_2) to remove any residual manganese dioxide present from previous experiments. The platinum was then mechanically polished by rubbing on a moist cloth coated with 1 μm alumina particles (2 min). After this the electrode was rinsed thoroughly with Milli-Q ultra pure water to remove any attached alumina particles before being patted dry with a lint-free tissue. The clean platinum electrode was then placed in the electrochemical cell together with the counter and reference electrodes, and the $MnSO_4/H_2SO_4$ electrolyte of choice that had previously been degassed with humid nitrogen gas for 10 min.

Chronoamperometry was used to electrodeposit manganese dioxide. To firstly identify suitable step voltages a linear sweep voltammogram of the platinum in the chosen electrolyte was conducted from the open circuit voltage up to 1.6 V at 5 mV s^{-1} using a Perkin–Elmer VMP 16-channel potentiostat controlled by EC-Lab software. From this voltammogram appropriate step voltages were chosen; two in the diffusion limited and two in the non-diffusion limited voltage range. Note the electrodeposition voltage is dependent on both the Mn^{2+} and acid concentrations in the electrolyte, and as such the chronoamperometric voltages chosen varied depending on the electrolyte. Once the step voltages had been determined the platinum electrode was cleaned and then returned to the electrodeposition cell. The chronoamperometry experiment was then conducted by stepping the platinum electrode voltage from the OCV to one of the previously identified step voltages for an appropriate time, typically 30 s. After this the coated platinum electrode was immediately removed from the electrochemical cell, rinsed thoroughly to remove entrained electrolyte with Milli-Q water, and then patted dry with a lint-free tissue. It was then immersed directly into a second similar electrochemical cell containing nitrogen purged 0.5 M Na_2SO_4 and allowed to equilibrate for 1 h under open circuit conditions. After this time the manganese dioxide electrode was cycled in the voltage range 0.0–0.8 V versus SCE at 5 mV s^{-1} for at least 50 cycles, again using a carbon counter electrode and an SCE reference electrode. For the purposes of comparison, an uncoated platinum electrode was also subjected to the same voltametric analysis.

3. Results and discussion

3.1. Voltametric behaviour

The potentiodynamic oxidation of Mn^{2+} to MnO_2 shows a conventional reversible anodic wave superimposed on the start of another wave corresponding to oxygen evolution. This was to be expected given the identical E° values for the two redox half-reactions [15]. E° for the MnO_2/Mn^{2+} redox couple assumes the thermodynamically stable β-MnO_2 as the manganese dioxide phase produced, although the literature indicates that metastable γ-MnO_2 was the phase produced under electrodeposition [16] which would have the effect of increasing the E° value.

The literature on manganese dioxide electrodeposition indicates that there are three potential mechanistic pathways that depend on the experimental conditions [17–23]; i.e., electrolyte composition (Mn^{2+} and H_2SO_4 concentration), temperature and current density. The first step in electrodeposition is accepted to be the oxidation of Mn^{2+} to Mn^{3+}. Following this, the behaviour of the Mn^{3+} in the electrolyte determines the predominant mechanistic pathway:

Path A: Soluble Mn^{3+} is metastable in a non-complexing aqueous media, hydrolysing to form solid MnOOH which precipitates on the electrode surface. The MnOOH can then undergo topotactic solid state oxidation to form MnO_2. This mechanism is preferred under conditions where soluble Mn^{3+} is unstable, such as in weakly acidic conditions. Furthermore, the structure of the MnOOH produced is anticipated to determine the resultant MnO_2 structure.

Path B: In this case the initial Mn^{2+} to Mn^{3+} oxidation process is followed by another one-electron oxidation process to form Mn^{4+}, which hydrolyses immediately to deposit MnO_2 on the electrode since soluble Mn^{4+} species in aqueous electrolytes without good complexing ligands have not been reported to exist [24]. The existence of this pathway is questionable given that there is no electrochemical evidence to show two sequential redox processes.

Path C: The final pathway occurs when the lifetime of the metastable Mn^{3+} produced in the first oxidation step is sufficiently long enough for it to react with another Mn^{3+} ion and disproportionate to form Mn^{2+} and Mn^{4+}, the latter of which hydrolyses

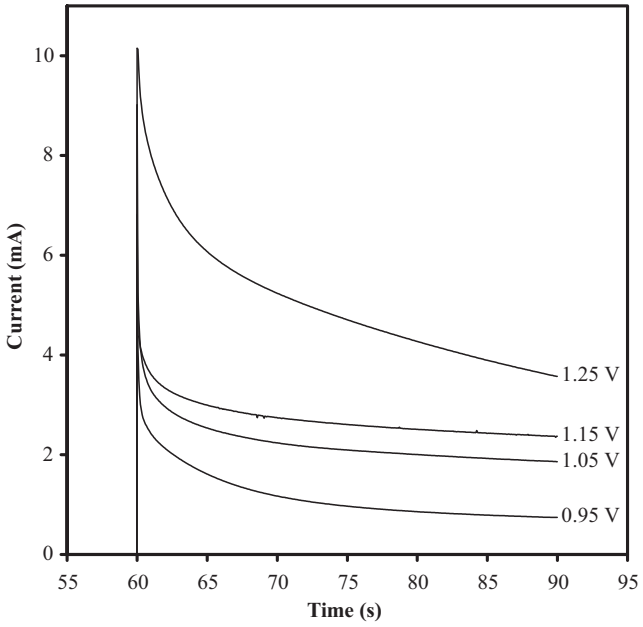

Fig. 1. Typical example of the resultant chronoamperometry data, in this case with an electrolyte of 0.1 M Mn^{2+} in 0.001 M H_2SO_4. The steps to 0.95 and 1.05 V were activation controlled, while the steps to 1.15 and 1.25 V were mass transport controlled.

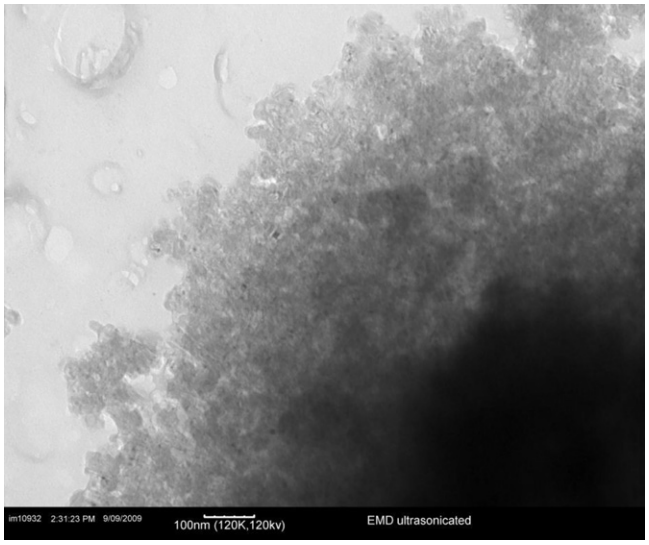

Fig. 2. TEM image of dried electrodeposited manganese dioxide scraped off the platinum substrate.

immediately to deposit MnO_2 on the electrode. This pathway is preferred in higher acid concentration electrolytes.

Despite these well delineated pathways, in reality a combination of these occurs to produce the resultant manganese dioxide [23]. As a final note it needs to be mentioned that the electrolyte conditions (via the predominant mechanism) also determine the resultant crystal structure and morphology of the manganese dioxide [25].

3.2. Chronoamperometry

From the voltametric data for each electrolyte, four step potentials were chosen; two below the peak voltage, in which case reaction kinetics are activation controlled, and two beyond the peak potential where reaction kinetics are mass transport controlled (predominantly diffusion, although in some instances migration would contribute). A typical example of the acquired chronoamperometry data is shown in Fig. 1, in this case for 0.1 M Mn^{2+} in 0.001 M H_2SO_4.

To compare electrode performance the mass of electrodeposited manganese dioxide needs to be determined. The approach we have chosen is to use numerical integration of the *i*–*t* data (Fig. 1) to determine the charge passed, which can then be converted into a mass. Using this approach the mass of electrodeposited manganese dioxide range from 5 to 70 μg depending on the deposition voltage and electrolyte used. These results were confirmed to within ± 10% by digesting the electrode into acidified H_2O_2, and then analysing the resulting solution by ICP-AES. Assuming a manganese dioxide density of 4.0 g cm^{-3} [26] and the formation of a dense deposit, 22.5 μg of MnO_2 would lead to an electrode thickness is ∼40 nm. There are many complications associated with this calculation including (i) the well-reported non-stoichiometric nature of manganese dioxide [27–29] (here foreign metal cations can be incorporated into the structure which will lead to and increase in electrode mass [27–31]); (ii) the hydration of manganese dioxide, which would also increase electrode mass [32]; (iii) the overlap of manganese dioxide electrodeposition with oxygen evolution, which would decrease the amount of active material present; and (iv) the apparent electrodeposition mechanism for manganese dioxide, which may lead to the loss of soluble manganese intermediates to the bulk electrolyte [23], which again would decrease the apparent mass. Morphologically, it is also unlikely that the manganese dioxide produced forms a dense deposit. Bulk electrodeposited manganese dioxide, as opposed to the thin films produced here, can have a BET surface area ranging from 10 to 100 m^2 g^{-1}, with the majority of this surface being associated with pores, in particular micro-pores [33]. This is particularly apparent in Fig. 2 which shows a TEM image of the dried manganese dioxide scraped off the platinum electrode surface. Under these circumstances it is highly likely that the thin films of material we have produced are quite porous, leading to a thicker deposit than predicted. Ultimately this porosity will be beneficial for supercapacitor performance because it allows for more surface area to be exposed to the electrolyte.

3.3. Cycling performance

After electrodeposition, the undried manganese dioxide-coated platinum electrodes were cycled potentiodynamically in 0.5 M Na_2SO_4 to evaluate their performance. The resultant voltametric data was as expected for a supercapacitive electrode material [4], exhibiting "rectangular" *i*–*V* behaviour that was retained, if not slightly increasing over the 50 cycles examined.

Fig. 3 contains specific capacitance data (as a function of chronoamperometric voltage, [Mn^{2+}] and [H_2SO_4]) for all the electrodes prepared. Immediately apparent is the very high specific capacitance for each electrode, calculated assuming that all charge during the chronoamperometry step was associated with the electrodeposition of manganese dioxide. The specific capacitance achieved far exceeds what has been previously reported in the literature [34]. Even within the range of errors introduced by the system features that would change the mass from its theoretical value, the capacitances achieved are substantial. The contributions made to the total measured capacitance from the bare platinum electrode were minimal (∼15 μF cm^{-2}) and so were ignored in the overall analysis. Considering the matrix of electrolytes considered, with their corresponding capacitance, we can conclude that the largest capacitance can be extract when a higher H_2SO_4 concentration and a lower Mn^{2+} concentration are used, and also when the step voltage is in the activation controlled region, rather than mass transport controlled.

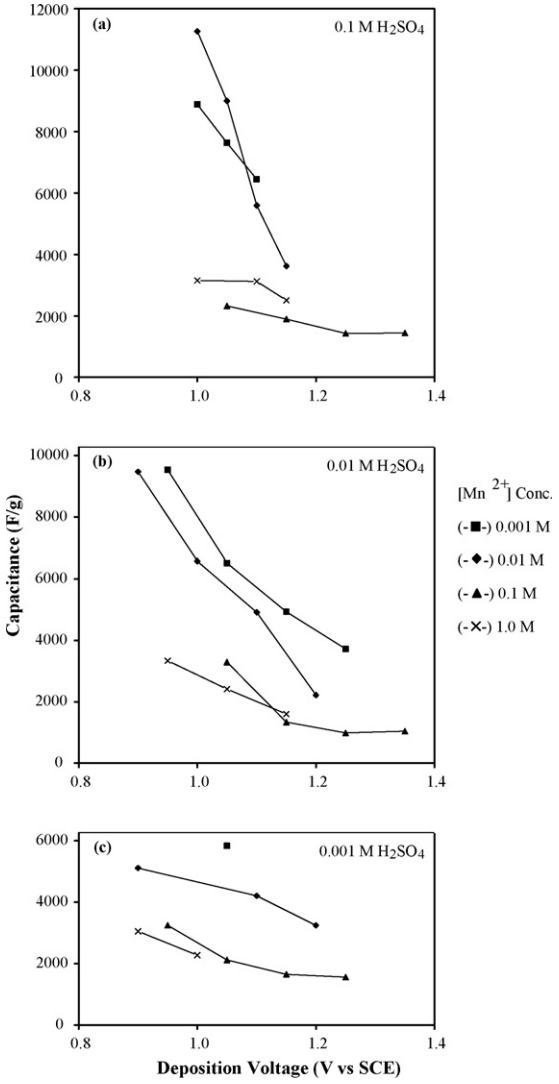

Fig. 3. Specific capacitance at the 50th cycle for the electrodeposited manganese dioxide samples as a function of H_2SO_4 concentration, Mn^{2+} concentration and deposition voltage.

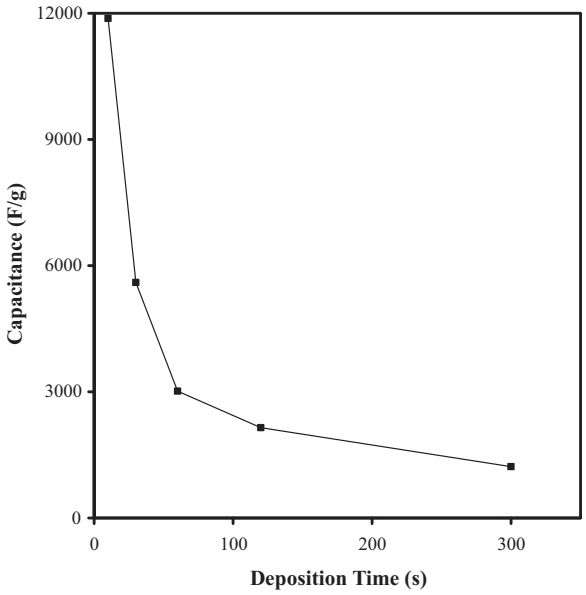

Fig. 4. Effect of deposition time on specific capacitance.

To explain this behaviour we must first assume that the specific surface area of the deposit accessible to the electrolyte is proportional to the extracted capacitance. This is reasonable given that all samples of electrodeposited manganese dioxide came from similar electrolytes, and so the chemistry of these materials is expected to be similar; i.e., there are no different foreign cations to influence the surface chemistry of one sample compared to another. Likewise, the crystal structure of the material is expected to be similar for the same reasons. Therefore, these electrodeposition conditions can be concluded to lead to the highest surface area deposit.

In higher H_2SO_4 concentration electrolytes the stability of the soluble Mn^{3+} intermediate has been shown to be greater [17–23], meaning that its lifetime is longer before either hydrolysis or disproportionation. Another consequence is that it provides a supporting electrolyte so that mass transport of the Mn^{2+} will be mostly by diffusion, rather than a combination of diffusion and migration which would make mass transport faster. Also, the use of a low Mn^{2+} concentration means that mass transport by diffusion to the electrode surface is again going to be relatively slow. When combined with an activation controlled deposition voltage, in which case the driving force for mass transport (activity gradient between the bulk electrolyte and the electrode surface) is again not as great, the rate of Mn^{2+} arrival at the electrode surface will again be slow. All these features of the system combined indicate that for the best performing electrode, and hence the highest surface area electrode, mass transport of the Mn^{2+} to the electrode surface must be as slow as possible. As a comment on the growth mechanism of the manganese dioxide, under these circumstances it would seem that crystal nucleation predominates so that the maximum surface area can be produced before the pores in the structure fill in to make a denser deposit.

To support these hypotheses, additional experiments were conducted using 0.01 M Mn^{2+} in 0.1 M H_2SO_4, an activation controlled step voltage, at both lower and higher temperatures compared to ambient (0 °C and 40 °C). At lower temperatures the diffusion coefficient for mass transport will be less, and vice versa at high temperatures. The resultant capacitances (14,033 F g^{-1} at 0 °C, 5600 F g^{-1} at 22 °C, and 3486 F g^{-1} at 40 °C) show quite clearly that slowing mass transport down by lowering the temperature has the effect of increasing the extracted capacitance, supporting our theory about mass transport and morphology. Additionally, it may also be possible for an increased temperature to increase the rate of crystal growth in the deposit as it is being formed. Of course this will also have the effect of decreasing the available specific surface area and hence capacitance.

Similar experiments were conducted to explore the mechanism of crystal growth during electrodeposition by depositing the manganese dioxide for different periods of time, followed by measuring the capacitance that can be extracted from the resulting electrode. Again using an electrolyte of 0.01 M Mn^{2+} in 0.1 M H_2SO_4, and an activation controlled step voltage, electrodeposition of manganese dioxide was carried out for various times ranging from 10 s up to 5 min. The resultant capacitance data is shown in Fig. 4. If the electrodeposition of manganese dioxide continued in the same fashion, as the deposition time increased then we should expect a constant specific capacitance. The fact that the capacitance decreases indicates that the available surface area is also decreasing with time. As mentioned above, after an analysis of the effects of the electrodeposition conditions, crystal nucleation apparently predominates during the initial stages of deposition. However, as time passes, rather than continuing to nucleate more crystals and increase the surface area, manganese dioxide is instead

deposited in such a fashion to fill up or close the pores, thus limiting the available surface area. This can be either by crystal growth of the initially deposited crystals, or by nucleation within the pores.

3.4. Comments on enhanced performance

The key feature of a supercapacitive electrode material is its ability to undergo fast reversible surface redox reactions [4]. The redox chemistry of manganese dioxide during electrochemical cycling is very rich with different reactions apparent when the material is in either acidic or basic electrolytes, or a combination of the two in neutral electrolytes, as we have used here. It is reasonable to assume that the manganese dioxide undergoes only a one-electron reduction, which in the bulk involves proton intercalation, and at the surface analogous metal ion (M^+) association; i.e.,

$$\text{Bulk + surface}: MnO_2 + H^+ + e^- \leftrightarrow MnOOH \quad (1)$$

$$\text{Surface}: MnO_2 + M^+ + e^- \leftrightarrow MnOOM \quad (2)$$

Due to size effects metals larger than H^+ and Li^+ cannot to any great extent be inserted into the manganese dioxide structure. The theoretical capacitance for this process is 1386 F g^{-1} assuming the starting material is stoichiometric manganese dioxide (this is almost always not the case, with the presence of lower valent manganese ions, cation vacancies and foreign metal ions lowering the stoichiometry [27–31]) and a voltage window of 0.8 V. Given that the capacitance we have measured is substantially higher than this, charge must be stored in some other fashion within the electrode. Of course there is the possibility of charge being stored in the double layer at the manganese dioxide–electrolyte interface, in series with the occurrence of fast redox processes. If this were to be the case then the surface area of our deposit is very high and/or the intrinsic charge storage capacity (F cm^{-2}) is larger than normal.

It is likely that the manganese dioxide electrodeposited during the course of our experiments has a large surface area, particularly given the relatively short timeframe over which the deposition was carried out. The evidence for this is apparent in Fig. 4 where the capacitance decreases with deposition time due to crystal nucleation within the existing pores effectively closing down the available surface area, as has been discussed above. If that were the case, then for a specific surface capacitance of say 15 μF cm^{-2} [35], and a total specific capacitance of 2000 F g^{-1}, the surface area is expected to be over 1.3×10^4 m^2 g^{-1}. Specific surface areas for manganese dioxide have never been reported to be this high [33], and so while our electrodeposited material may very well have a higher surface area, it is not realistic to assume that it is this high. The value used for the surface specific capacitance in the preceding calculation is typical for many metal (and carbon) electrode–electrolyte systems [35]. However, it may not be appropriate for metal oxide systems in which case the structure and polarity of the oxide groups at the surface are expected to be significantly different. To demonstrate this, consider that a typical specific capacitance values reported in the literature for manganese dioxide is ~180 F g^{-1} for a material with a specific surface area (BET) of ~120 m^2 g^{-1} [6]. This equates to a specific surface capacitance of ~150 μF cm^{-2}, which is an order of magnitude higher than that assumed for a metal electrode. Assuming this value and revisiting the previous calculation, the specific surface area turns out to be ~1300 m^2 g^{-1}, which, while high, is not unreasonable. The question then becomes what is the source of this enhanced specific capacitance?

In previous work from our laboratory we have shown that the surface of manganese dioxide in an aqueous environment consists of a relatively high concentration of surface hydroxyl groups that exhibit amphoteric behaviour [36,37]; i.e.

$$\equiv Mn - OH_2^+ \cdot X^- + OH^- \overset{\pm(H_2O+X^-)}{\underset{K_b}{\longleftrightarrow}}$$

$$\equiv Mn - OH \overset{\pm(M^+)}{\underset{K_a}{\longleftrightarrow}} \equiv Mn - O^- \cdot M^+ + H^+ \quad (3)$$

where K_a and K_b are the acidic and basic equilibrium constants, and X^- and M^+ are generic anionic and cationic counter charges. Whether the surface behaves in an acid or basic fashion is determined by the underlying crystal structure of the manganese dioxide, while the specific sites function depending on K_a and K_b, and the pH of the electrolyte in which the manganese dioxide is immersed, in which case the hydroxyl groups either release or abstract a proton to or from the electrolyte, respectively. The point being made is that these surface hydroxyl groups are charge storage sites, and instead of using the solution pH as a means to activate or deactivate the surface, the electrode potential can be used instead. For instance, if the electrode potential were made more negative (cathodic) the surface hydroxyl groups on the manganese dioxide can be polarized so that they can abstract a proton or metal ion from the electrolyte as a means of charge balance. This process is of course dependent on the conductivity of the manganese dioxide since the charge applied to the electrode has to find its way to the manganese dioxide–electrolyte interface without incurring significant ohmic polarization. Furthermore, the conductivity of manganese dioxide (γ-MnO_2) has been reported [38] to decrease substantially (~5 order of magnitude), at least in bulk form, when reduced. Nevertheless, based on the fact that we are using nanoscale deposits, in which case the conduction path lengths are much shorter than in the bulk, material conductivity may not be an issue. Given the voltammograms we have measured were typical for an ideal supercapacitor electrode, low conductivity or conductivity changes are apparently not significant.

To estimate the specific surface charge using this model we must refer back to the crystal structure of the manganese dioxide. Assuming that the electrodeposited phase is γ-MnO_2 (orthorhombic symmetry with a_0 = 9.32 Å, b_0 = 4.46 Å and c_0 = 2.85 Å and N = 4 [30,31]), we can calculate the surface area of one formula unit (A_f; m^2) using

$$A_f = \frac{2(a_0b_0 + a_0c_0 + b_0c_0)}{N} \quad (4)$$

Assuming stoichiometric MnO_2, this area is therefore associated with two oxygen ions, both of which are assumed to be associated with the formation of surface hydroxyl groups, thus giving the surface area per oxygen ion (A_O; m^2); i.e.

$$A_O = \frac{A_f}{2} \quad (5)$$

Now, the surface capacity (Q_{OH}; C m^{-2}) can be calculated using

$$Q_{OH} = \frac{q_O}{A_O} \quad (6)$$

where q_O is the charge on an oxygen ion at the surface. If we assume that q_O is the same as the electron charge ($q_e = 1.6 \times 10^{-19}$ C), then the total capacitance associated with the manganese dioxide surface is given by

$$C_T = \frac{Q_{OH}}{V} \quad (7)$$

where V is the voltage window (assumed to be 0.8 V). Under these circumstances C_T calculates to be ~100 μF cm^{-2}, which certainly shows the potential that surface hydroxyl groups can contribute to the overall capacitance. Points to note include:

(i) This calculation assumes that each individual unit cell is exposed to the electrolyte, which is of course not possible. Assuming a cluster of unit cells to produce a regular 10 nm × 10 nm × 10 nm crystal (~800 unit cells, ~3200 formula units), the available area will decrease by ~20 times, meaning the surface capacitance will drop to ~5 μF cm^{-2}. Of course if the crystal produced is a needle or lathe, then this will influence the unit cell faces exposed to the electrolyte and hence also the hydroxyl group surface density.
(ii) The assumption was also made that all oxide anions are able to form hydroxyl groups. This is reasonable given the ability of manganese to form an aquo-complex in solution [24], and also the intrinsic polarization of the $Mn^{\delta+}$–$O^{\delta-}$ bond [36,37].
(iii) This bond polarity will also influence the assumption that a surface oxide ion can be fully associated with the electronic charge; i.e., the bond between manganese and oxygen is assumed to essentially be ionic in nature, which is certainly not the case. The covalency of the bond between manganese and oxygen will act to decrease the total charge available to each oxygen ion (q_O), and hence the total capacitance (C_T). At this time an estimate for this effect is unavailable.

As a final point a comment needs to be made concerning the overall performance characteristics of supercapacitor devices that would use the materials described in this work. From a purely material performance perspective, for a thin film of electrodeposited manganese dioxide produced in this work that exhibits a specific capacitance of 2000 F g^{-1} over a 0.8 V window using a potential scan rate of 5 mV s^{-1}, the specific energy and power densities are 350 Wh kg^{-1} and 8000 W kg^{-1}, respectively. This places these materials superior to Li primary cells in terms of energy density, as well as being at the upper range of supercapacitor power density despite the use of a rather slow scan rate [3]. Of course when the materials are used in real cells the performance decreases due to the presence of inactive (but essential) materials such as the cell body, substrate, electrolyte and separator. To estimate the contributions to the overall performance of the inactive cell components is difficult at this stage of cell development; however, if the active materials contributed ~2% of the total cell mass, then this would leave them being equal with the current best performing supercapacitors in terms of specific energy density (~8 Wh kg^{-1}). In terms of power density incorporating the mass of inactive materials will also decrease overall cell performance within the supercapacitor domain in the Ragone diagram [3]. However, the present data set only uses a low cycling rate, and certainly if we were to increase this it would improve cell power density.

4. Summary and conclusions

In this work chronoamperometry has been used to prepare thin films of electrodeposited manganese dioxide (estimated to be 20–100 nm thick) from an electrolyte consisting of $MnSO_4$ and H_2SO_4. Evaluation of these materials as supercapacitor electrodes in 0.5 M Na_2SO_4 shows that they possess excellent specific capacitances, in some instances 10–20 times greater than literature data. Specific outcomes from the work include:

(i) From the matrix of $MnSO_4$ and H_2SO_4 electrolytes used to electrodeposit the manganese dioxide the most active supercapacitor electrode materials were produced using an activation controlled potential rather than a diffusion controlled potential, suggesting that a high surface area morphology is obtained under these conditions.
(ii) This conclusion was further supported by electrodeposition experiments conducted at different temperatures, with a clear improvement in performance resulting from an electrode made at a lower temperature where mass transport is slowed down even further.
(iii) Normalization of our data (in terms of performance per gram of active material) was achieved by using the charge passed during electrodeposition to calculate the amount of manganese dioxide deposited. Complications associated with this approach, such as the non-stoichiometric nature of the deposit, and the presence of water and foreign cations, were also considered. Confirmation of this approach as being acceptable was carried out by dissolving the deposit and measuring the amount of manganese released into solution.
(iv) The enhanced specific capacitance of these electrodes was discussed in terms of faradaic and non-faradaic contributions, as well as in terms of the number of active adsorption sites on the manganese dioxide surface.

Acknowledgements

The authors acknowledge the funding provided by the CSIRO Division of Energy Technology and the University of Newcastle to conduct this research.

Appendix A. Supplementary data

Supplementary data associated with this article can be found, in the online version, at doi:10.1016/j.jpowsour.2011.04.049.

References

[1] N.S. Lewis, Scientific Challenges in Sustainable Energy Technology, Plenary Lecture 208th Meeting of the Electrochemical Society, Los Angeles CA USA, October, 2005.
[2] D. Ragone, Proc. Soc. Automotive Engineers Conference, Detroit MI USA, May, 1968.
[3] P. Simon, Y. Gogotsi, Nat. Mat. 7 (2008) 845–854.
[4] B.E. Conway, Electrochemical Supercapacitors: Scientific Fundamentals and Technological Applications, Kluwer-Plenum Publishing Company, New York, 1999.
[5] K. Naoi, P. Simon, Electrochem. Soc. Interface 17 (2008) 34–37.
[6] D. Bélanger, T. Brousse, J.W. Long, Electrochem. Soc. Interface 17 (2008) 49–52.
[7] W. Feitknecht, W. Marti, Helv. Chim. Acta 28 (1945) 129–148.
[8] W. Feitknecht, W. Marti, Helv. Chim. Acta 28 (1945) 149–156.
[9] O. Glemser, G. Gattow, H. Meisiek, Z. Anorg. Allg. Chem. 309 (1961) 1–19.
[10] Y.F. Yao, N. Gupta, H.S. Wroblowa, J. Electroanal. Chem. Interface Electrochem. 223 (1987) 107–117.
[11] R.M. McKenzie, Miner. Magn. 38 (1971) 493–502.
[12] J.B. Fernandes, B.D. Desai, V.N. Kamat Dalal, J. Power Sources 15 (1985) 209–237.
[13] E. Narita, T. Okabe, Bull. Chem. Soc. Jpn. 53 (1980) 525–532.
[14] M.H. Rossouw, D.C. Liles, M.M. Thackeray, Prog. Batt. Batt. Mater. 15 (1996) 8–18.
[15] M. Pourbaix, Atlas of Electrochemical Equilibria in Aqueous Solutions, National Association of Corrosion Engineers, Houston, USA, 1974.
[16] C.B. Ward, A.I. Walker, A.R. Taylor, Prog. Batt. Batt. Mater. 11 (1992) 40–46.
[17] M. Fleischmann, H.R. Thirsk, I.M. Tordesillas, Trans. Faraday Soc. 58 (1962) 1865–1877.
[18] A. Cartwright, R.L. Paul, in: B. Schumm, H.M. Joseph, A. Kozawa (Eds.), Proc. MnO_2 Symposium, Volume 2, Tokyo, 1980, pp. 290–304.
[19] R.L. Paul, A. Cartwright, J. Electroanal. Chem. Interface Electrochem. 201 (1986) 113–122.
[20] R.L. Paul, A. Cartwright, J. Electroanal. Chem. Interface Electrochem. 201 (1986) 123–131.
[21] E. Preisler, in: K.V. Kordesch, A. Kozawa (Eds.), Proc. 2nd Battery Materials Symposium, Volume 2, Graz, 1985, pp. 247–266.
[22] W.H. Kao, V.J. Weibel, J. Appl. Electrochem. 22 (1992) 21–27.
[23] C.J. Clarke, G.J. Browning, S.W. Donne, Electrochim. Acta 51 (2006) 5773–5784.
[24] Cotton S F.A., Wilkinson S G., Murillo S C.A., Bochmann S M., Advanced Inorganic Chemistry, 6th ed., John Wiley and Sons, 1999.
[25] R. P. Williams, Characterisation and Production of High Performance Electrolytic Manganese Dioxide for Use in Primary Alkaline Cells, PhD Thesis, University of Newcastle (1995).
[26] D.A.J. Swinkels, K.N. Hall, Prog. Batt. Batt. Mater. 11 (1992) 16–24.
[27] P. Ruetschi, R. Giovanoli, J. Electrochem. Soc. 135 (1988) 2663–2669.
[28] P. Ruetschi, J. Electrochem. Soc. 135 (1988) 2657–2663.
[29] P. Ruetschi, J. Electrochem. Soc. 131 (1984) 2737–2744.
[30] V.M. Burns, R.G. Burns, W.K. Zwicker, in: A. Kozawa, R.J. Brodd (Eds.), Proc. MnO_2 Symp., Vol. 1, 1975, pp. 288–305.

[31] R.G. Burns, V.M. Burns, in: A. Kozawa, R.J. Brodd (Eds.), Proc. MnO_2 Symp., Vol. 1, 1975, pp. 306–327.
[32] D.K. Walanda, G.A. Lawrance, S.W. Donne, J. Power Sources 139 (2005) 325–341.
[33] J.B. Arnott, R.P. Williams, A.G. Pandolfo, S.W. Donne, J. Power Sources 165 (2007) 581–590.
[34] S.C. Pang, M.A. Anderson, T.W. Chapman, J. Electrochem. Soc. 147 (2000) 444–450.
[35] J.O'M. Bockris, A.K.N. Reddy, Modern Electrochemistry, Plenum Publishing Corporation, New York, 1970.
[36] A.P. Malloy, G.J. Browning, S.W. Donne, J. Colloid Interface Sci. 285 (2005) 653–664.
[37] A.P. Malloy, S.W. Donne, J. Colloid Interface Sci. 320 (2008) 210–218.
[38] X. Xia, H. Li, Z.H. Chen, J. Electrochem. Soc. 136 (1989) 266–271.